

# UCSF

## UC San Francisco Previously Published Works

### Title

Unraveling the Biology of a Fungal Meningitis Pathogen Using Chemical Genetics

### Permalink

<https://escholarship.org/uc/item/0hm9v75k>

### Journal

Cell, 159(5)

### ISSN

0092-8674

### Authors

Brown, Jessica CS  
Nelson, Justin  
VanderSluis, Benjamin  
[et al.](#)

### Publication Date

2014-11-01

### DOI

10.1016/j.cell.2014.10.044

Peer reviewed

Published in final edited form as:

*Cell*. 2014 November 20; 159(5): 1168–1187. doi:10.1016/j.cell.2014.10.044.

## Unraveling the biology of a fungal meningitis pathogen using chemical genetics

Jessica C. S. Brown<sup>1,6</sup>, Justin Nelson<sup>2</sup>, Benjamin VanderSluis<sup>2</sup>, Raamesh Deshpande<sup>2</sup>, Arielle Butts<sup>3</sup>, Sarah Kagan<sup>4</sup>, Itzhack Polacheck<sup>4</sup>, Damian J. Krysan<sup>3,5</sup>, Chad L. Myers<sup>2,7</sup>, and Hiten D. Madhani<sup>1,7</sup>

<sup>1</sup>Department of Biochemistry and Biophysics, University of California, San Francisco, CA 94158, USA

<sup>2</sup>Department of Computer Science and Engineering, University of Minnesota, Minneapolis, MN 55455, USA

<sup>3</sup>Department of Chemistry, University of Rochester Medical Center, Rochester, NY 14643, USA

<sup>4</sup>Department of Clinical Microbiology and Infection Diseases, Hadassah-Hebrew University Medical Center, Jerusalem, Israel

<sup>5</sup>Departments of Pediatrics and Microbiology/Immunology, University of Rochester School of Medicine and Dentistry, Rochester, NY 14643, USA

### Summary

The fungal meningitis pathogen *Cryptococcus neoformans* is a central driver of mortality in HIV/AIDS. We report a genome-scale chemical genetic data map for this pathogen that quantifies the impact of 439 small molecule challenges on 1448 gene knockouts. We identified chemical phenotypes for 83% of mutants screened and at least one genetic response for each compound. *C. neoformans* chemical-genetic responses are largely distinct from orthologous published profiles of *Saccharomyces cerevisiae*, demonstrating the importance of pathogen-centered studies. We used the chemical-genetic matrix to predict novel pathogenicity genes, infer compound mode-of-action, and to develop an algorithm, O2M, that predicts antifungal synergies. These predictions were experimentally validated, thereby identifying virulence genes, a molecule that triggers G2/M arrest

© 2014 Elsevier Inc. All rights reserved.

<sup>7</sup>corresponding authors: cmyers@cs.umn.edu, hitenmadhani@gmail.com.

<sup>6</sup>Present address: Department of Pathology, Division of Microbiology and Immunology, University of Utah School of Medicine, Salt Lake City, UT 84112, USA

### Author Contributions

J.C.S.B. and H.D.M. designed the study. J.C.S.B. carried out all of experiments described in the paper. J.N. and C.L.M. performed data analysis shown in Figs. 1B–D, Fig. 2 and Fig. 3. B.V., R.D., and C.L.M. filtered, de-noised and scored the primary colony array data. A.B., S.K., I.P., and D.J.K. provided compounds and guidance. J.C.S.B. and H.D.M. wrote the manuscript with input from all co-authors.

### SUPPLEMENTAL MATERIAL

Supplemental Material includes Extended Experimental Procedures, Literature References for Table 1, three supplementary figures and seven supplementary tables.

**Publisher's Disclaimer:** This is a PDF file of an unedited manuscript that has been accepted for publication. As a service to our customers we are providing this early version of the manuscript. The manuscript will undergo copyediting, typesetting, and review of the resulting proof before it is published in its final citable form. Please note that during the production process errors may be discovered which could affect the content, and all legal disclaimers that apply to the journal pertain.

and inhibits the Cdc25 phosphatase, and many compounds that synergize with the antifungal drug fluconazole. Our work establishes a chemical-genetic foundation for approaching an infection responsible for greater than one-third of AIDS-related deaths.

---

## Introduction

Invasive fungal infections are notoriously difficult to diagnose and treat, resulting in high mortality rates, even with state-of-the-art treatments. The three most common pathogenic agents are *Cryptococcus neoformans*, *Candida albicans*, *Aspergillus fumigatus* (Mandell *et al.*, 2010). These organisms are opportunistic fungi that prey on individuals with varying degrees of immune deficiency. Susceptible patient populations include premature infants, diabetics, individuals with liver disease, chemotherapy patients, organ transplant recipients, and those infected with HIV (Mandell *et al.*, 2010). Compounding the clinical challenge is the slow pace of antifungal drug development: only a single new class of drugs (the echinocandins) has been approved for use in the United States in the last 30 years (Butts and Krysan, 2012; Mandell *et al.*, 2010; Roemer *et al.*, 2011).

Fungal infections are estimated to cause 50% of deaths related to Acquired Immunodeficiency Syndrome (AIDS), and have been termed a “neglected epidemic” (Armstrong-James *et al.*, 2014). The fungus chiefly responsible for deaths in this population is *Cryptococcus neoformans* (Armstrong-James *et al.*, 2014). *C. neoformans* is an encapsulated basidiomycetous haploid yeast distantly related *Saccharomyces cerevisiae* and *Schizosaccharomyces pombe*. A 2009 CDC study estimated that ~1 million infections and ~600,000 deaths annually are caused by *Cryptococcus neoformans*, exceeding the estimated worldwide death toll from breast cancer (Lozano *et al.*, 2012; Park *et al.*, 2009). *Cryptococcus neoformans* is widespread in the environment and exposure occurs through inhalation of desiccated yeast or spores (Heitman *et al.*, 2011). In immunocompromised patients, *C. neoformans* replicates and disseminates, causing meningoencephalitis that is lethal without treatment (Heitman *et al.*, 2011). Induction therapy involves flucytosine and intravenous infusions of amphotericin B (Loyse *et al.*, 2013). Both drugs are highly toxic, difficult to administer, and neither is readily available in the areas with the highest rates of disease. The current recommendation for cryptococcosis treatment is at least a year of therapy, which is difficult to accomplish in resource-limited settings (WHO, 2011). Thus, as is the case with infections caused by other fungal pathogens, effective treatment of cryptococcal infections is limited by the efficacy, toxicity, and availability of current pharmaceuticals.

We implemented chemogenomic profiling to approach the challenges of therapeutic development in *C. neoformans*. This method involves the systematic measurement of the impact of compounds on the growth of defined null mutants to produce a chemical-genetic map. Such a map represents a quantitative description composed of numerical score indicative of the growth behavior of each knockout mutant under each chemical condition. Cluster analysis of the growth scores for large numbers of mutants under many chemical conditions can reveal genes that function in the same pathway and even those whose products are part of the same protein complex (Collins *et al.*, 2007; Parsons *et al.*, 2004;

Parsons et al., 2006). In addition, the identity of genes whose mutation produce resistance or sensitivity is useful for uncovering compound mode-of-action (MOA) (Hillenmeyer *et al.*, 2008; Jiang *et al.*, 2008; Nichols *et al.*, 2010; Parsons *et al.*, 2006; Xu *et al.*, 2007; Xu *et al.*, 2009). Large-scale studies have been restricted to model organisms for which gene deletion collections have been constructed, namely *S. cerevisiae*, *S. pombe*, and *Escherichia coli* K12 (Hillenmeyer *et al.*, 2008; Nichols *et al.*, 2010; Parsons *et al.*, 2006). However, as none of these are pathogens, the extent to which the resulting insights translate to pathogenic organisms is unknown. A variation on chemogenomic profiling, chemically-induced haploinsufficiency, was first developed using a diploid heterozygote gene deletion library *S. cerevisiae* to identify compound MOA. This method, which identifies genes that impact compound sensitivity based a two-fold gene dosage change, is suited for diploid organisms and has been used in the pathogen *C. albicans* (Jiang *et al.*, 2008; Xu *et al.*, 2007; Xu *et al.*, 2009).

We report here the generation of a large-scale chemogenomic map for *C. neoformans* using defined, commonly available knockout mutants, assessments of data quality, and extensive experimental verification. Comparisons of the *C. neoformans* profile with two large-scale published profiles from *S. cerevisiae* revealed that for most types of compounds, the chemical-genetic interactions are distinct even among orthologous genes, emphasizing the importance of pathogen-focused investigation. We used nearest-neighbor analysis to predict new genes involved in polysaccharide capsule formation and infectivity, which we validated through experiment. We also utilized genetic responses to predict the G2/M phase of the cell cycle and the Cdc25 phosphatase as targets of a thiazolidone-2,4-dione derivative, which we confirmed *in vivo* and *in vitro*. Finally, because of the unmet need for improved antifungal drug efficacy, we developed a new algorithm, O2M, to predict new compound synergies based on the profiles of pairs known to be synergistic. Experimental tests demonstrate that the method performs vastly better than random expectation, thereby enabling the identification of synergistic compound combinations. Our studies establish a chemical-genetic foundation to approach the biology and treatments *C. neoformans* infections, which are responsible for more than one-third of HIV/AIDS deaths worldwide.

## Results

### A chemical-genetic map of *C. neoformans*

We assembled 1448 *Cryptococcus neoformans* gene deletion strains (Chun *et al.*, 2011; Liu *et al.*, 2008) (Table S1), corresponding to a substantial fraction of 6,967 predicted *C. neoformans* genes (Janbon *et al.*, 2014), and a collection of compounds for screening (Table 1). Compounds were selected based on cost and literature evidence that they could inhibit the growth of fungi. Where feasible, compounds were chosen that are known to target specific biological processes. For each small molecule, we determined an approximate minimum inhibitory concentration (MIC) in agar, then measured growth of the knockout collection on each small molecule at 50%, 25%, and 12.5% MIC using high density agar plate colony arrays and a robotic replicator. We then measured the size of each colony using flatbed scanning and colony measurement software (Dittmar *et al.*, 2010). We performed a minimum of four replicate colony measurements for each mutant-condition pair. Plate-based

assays are subject to known non-biological effects, such as spatial patterns. To mitigate these errors, a series of corrective measures were implemented using approaches described previously, including manual filtration of noisy data, spatial effect normalization and machine learning-based batch correction (Baryshnikova *et al.*, 2010). In addition, the data for each deletion mutant and compound was centered and normalized. Each mutant-small molecule combination was assigned a score with positive scores representing relative resistance and negative scores representing compound sensitivity (Table S2). A global summary of the processed data organized by hierarchical clustering is shown in Fig. 1A.

The importance and validity of the computational corrections is shown in Fig. 1B and Fig. S1. We estimated how reproducible the chemical-genetic profiles were by calculating the correlation scores for data obtained for different concentrations of the same small molecule (purple). This measures the degree of overlap between the overall chemical-genetic profiles, which are themselves each composed of a score for each mutant-small molecule combination. We found significant correlation ( $p = 2.67 \times 10^{-176}$ ) between data obtained for different concentrations of the same small molecule compared to those between profiles generated by dataset randomization, suggesting significant reproducibility. Moreover, correlation scores between chemical-genetic profiles of different concentrations of different compounds (gray) are centered at approximately zero (Fig. 1B). This difference in correlation scores is apparent even when comparing experiments performed on the same day, when spurious batch signal can contribute to false positives (Baryshnikova *et al.*, 2010). Our batch-correction algorithms resulted in same-batch screening data with strong positive correlation scores for the same compounds but correlation scores close to zero for different compounds (Fig. S1), demonstrating successful removal of spurious signal (Baryshnikova *et al.*, 2010). We compared chemical-genetic profiles between compounds in the azole family (Fig. 1C). Despite the fact that the azoles tested includes those of diverse uses, from agricultural pesticides to FDA-approved drugs (Table 1), many exhibit a significant profile correlation ( $p = 2.82 \times 10^{-6}$ ), further indicating significant signal in the data. As a final assessment, we performed hypergeometric testing across all compounds to determine whether the same sensitive gene knockouts (defined by  $Z < -2.5$ ) are identified at different concentrations of the same compounds. Using a Bonferroni-corrected p-value cutoff, nearly all compounds display significant overlap of responsive genes at different concentrations (Fig. 1D).

We assigned at least one phenotype (sensitivity or resistance to a compound) to 1198 of 1448 mutants (Fig. 1E, Table S2–S4). Of these, 855 exhibit one to ten phenotypes, while remaining 343 displayed from 11 to 146 phenotypes. Gene deletions with the greatest number of phenotypes are *cnag\_07622* (encoding the COP9 signalosome subunit 1) and *cnag\_05748* (encoding a N to 1 subunit of the NuA3 histone acetyltransferase). Compounds that elicit the greatest number of responsive gene deletions (Fig. 1F) are the heavy metal salt sodium tungstate and the trichothecene protein synthesis inhibitor verrucarin (Table S5), presumably reflecting the pleiotropic impact of these molecules on cells.

## Gene Ontology analysis reveals processes associated with drug sensitivity

Drug influx and efflux is thought to be a major general determinant of microbial drug susceptibility (Fernández and Hancock, 2012), but we also sought functions involved in drug sensitivity. We investigated this question in an unbiased fashion by analyzing chemogenomic profiles using Gene Ontology (GO), a gene annotation approach useful for comparative analyses. We first identified annotated orthologs of *C. neoformans* genes represented in the deletion library and associated GO terms with these orthologs. We then determined whether the sensitive gene knockouts that respond to each small molecule are enriched for association with particular GO terms relative to a randomized control set (Fig. 2, Table S6). We observed that protein transport-related terms are highly enriched, as are processes related to ubiquitin modification/proteolysis and vesicle-mediated transport. These terms are associated with nine and five compounds, respectively, suggesting that intracellular transport and ubiquitin-mediated protein turnover may play important general roles in drug sensitivity.

## Comparison with *S. cerevisiae* chemogenomic profiling datasets

Chemogenomic profiling has been performed extensively in *S. cerevisiae*, allowing us to ask whether genetic responses to compounds were conserved. We performed a three-way comparison with two large-scale studies (Hillenmeyer *et al.*, 2008; Parsons *et al.*, 2006) (Fig. 3A). Our dataset has 46 compounds in common with Parsons *et al.* and 29 with Hillenmeyer *et al.*; the two *S. cerevisiae* datasets had 15 compounds in common. First we identified genes whose knockouts exhibited a significant ( $Z = -2.5$  or  $+2.5$ ) score (“responding”) when treated with a small molecule used in more than one dataset, then identified which of those genes had orthologs in both *S. cerevisiae* and *C. neoformans*. We then calculated how many orthologs responded in both datasets. To adjust for a greater starting number of common genes when comparing the *S. cerevisiae* datasets to each other and control for functional biases, we limited this comparison to genes that also have orthologs in the *C. neoformans* knockout collection. The blue labels for compounds in Fig. 3B–D indicate statistically significant similarities ( $p < 0.05$ ) in drug responses. Nearly all of the compounds in common between the two *S. cerevisiae* studies display statistically significant overlap in the genes that produced sensitivity to a given compound, despite the very different experimental platforms were used to assess drug sensitivity/resistance (13/15 cases; Fig. 3B). In striking contrast, few compounds show significantly conserved genetic responses when comparing either *S. cerevisiae* dataset with the *C. neoformans* data. For the two *C. neoformans*-*S. cerevisiae* comparisons, only two of 46 compounds (Fig. 3C) and one of 29 compounds (Fig. 3D) show conserved responses, respectively.

The responses to azole compounds exhibit limited response conservation between species. Comparing our dataset with Parsons *et al.*, the responses to fluconazole (FLC) and clotrimazole, the azoles in both datasets, do not show significant overlap (Fig. 3C). Likewise, between our dataset and Hillenmeyer *et al.*, no gene orthologs respond to miconazole and clotrimazole in both datasets (Fig. 3D). In contrast, between the two *S. cerevisiae* datasets, the only shared azole, clotrimazole, shows a significantly similar response (Fig. 3B). We compared published work that examined the transcriptome responses of *S. cerevisiae* (Kuo *et al.*, 2010) and *C. neoformans* (Florio *et al.*, 2011) to FLC. We found

that, while there was significant overlap in orthologous genes impacted in the two species, ( $p = 1.6 \times 10^{-3}$ ), there were also considerable differences: 67% of the genes with an altered response in *C. neoformans* whose orthologs in *S. cerevisiae* did not exhibit significant change. (Table S7) (Kuo et al., 2010).

### Using chemical-genetic signatures to identify capsule biosynthesis mutants

Studies in *S. cerevisiae* have shown that that the phenotypic signatures of gene deletions for genes that act in the same process or protein complex tend to be similar (Collins *et al.*, 2007; Costanzo *et al.*, 2010; Nichols *et al.*, 2010; Parsons *et al.*, 2004; Parsons *et al.*, 2006). We reasoned that this property of could be used in a pathogen to identify candidates for new genes involved in virulence by simply testing gene deletions that displayed phenotypic profiles similar to those corresponding to known virulence factors.

*C. neoformans* harbors an inducible polysaccharide capsule that is unusual among fungi (Del Poeta, 2004; Doering, 2009; Haynes *et al.*, 2011; Kumar *et al.*, 2011; O'Meara and Alspaugh, 2012; O'Meara *et al.*, 2010; Vecchiarelli *et al.*, 2013). The principal polysaccharide component, glucuronylxylomannan (GXM), consists of repeating glycan unit that has  $\alpha$ -1,3-linked mannose backbone with side chains of  $\beta$ -linked glucuronic acid and xylose (Kozel *et al.*, 2003). Capsule production is critical for virulence and the ability of *C. neoformans* to evade detection and destruction by the host immune system (Vecchiarelli *et al.*, 2013).

To identify candidates for genes involved in capsule formation and/or attachment, we organized our dataset using hierarchical clustering of growth phenotypes produced by compound exposure. We focused on two clusters, each containing a gene(s) previously implicated in capsule biosynthesis: *PBX1* and *CPL1* (Liu *et al.*, 2008; Liu *et al.*, 2007b) in one cluster (Fig. 4A) and *CAP60* (Chang and Kwon-Chung, 1998) in a second cluster (Fig. 4B). The *pbx1 /cpl1* cluster contains nine genes and the *cap60* cluster seven. We quantified capsule accumulation after induction by computing the ratio of the diameter of the cell and capsule to the diameter of the cell alone (Fig. 4C, Fig. 4D). Wild-type cells exhibit high capsule production, *pbx1* mutants display a partial defect (Liu *et al.*, 2007a) and *cpl1* and *cap60* mutants are acapsular (Chang and Kwon-Chung, 1998; Liu *et al.*, 2008). We found that seven of nine mutants in the *pbx1 /cpl1* cluster exhibit a statistically significant capsule defect, as did four of the seven mutants in the *cap60* cluster. In contrast, previous work from our laboratory found that approximately 1% of the original *C. neoformans* library shows a gross defect in capsule production (Liu *et al.*, 2008).

Previous work showed that *pbx1* mutants produce polysaccharide capsule whose attachment to the cell wall is sensitive to sonication, a finding that we confirmed (Fig. 4C, D). We refer to the cell's ability to retain GXM on the cell surface as "capsule maintenance." Knockout mutants in *cnag\_01058* do not exhibit a basal capsule defect but lost nearly 40% of their capsule diameter following sonication. Cells deleted for the *GCN5* gene, like *pbx1* cells, show both decreased capsule levels and sonication-sensitive capsule. None of the mutants from the *cap60* cluster produces a sonication-sensitive phenotype, suggesting that the *pbx1 /cpl1* and *cap60* clusters organize mutants that have distinct phenotypes. However, because several mutants do not produce visible capsule, the

sonication test is insufficient to definitively measure capsule maintenance. We therefore analyzed how much glucuronoxylomannan (GXM), the major capsular polysaccharide (Doering, 2009), is secreted into the growth medium by blotting with  $\alpha$ -GXM antibodies (Fig. S2A). We found that two mutants that produce little (*gcn5*) or no (*yap1*) visible capsule still shed GXM into the medium, suggesting that they cannot retain capsule on their cell surface. Indeed, we found that they shed more GXM than *pbx1* cells. Four of nine mutants in the *pbx1* /*cpl1* cluster exhibit a maintenance defect, whereas none of the *cap60* cluster mutants do. We also found that GXM produced by these cells can be taken up and added to the surface (“donated”) of an acapsular mutant using a standard GXM transfer assay (Kozel and Hermerath, 1984; Reese and Doering, 2003). Moreover, apparent capsule-defective mutants shed GXM (Fig. S2B, C) and can donate GXM from conditioned medium (Fig. S2C). Mutants that appear to not secrete GXM (*pbx1*, *cpl1*, and *sgf73*) can donate it, but only if conditioned medium concentration is increased 10-fold (Fig. S2D). These data are consistent with a recently published study on the role of Pbx1 in capsule attachment and assembly (Kumar *et al.*, 2014).

Since the capsule is a major virulence trait of *C. neoformans*, we tested whether knockout mutants that exhibited a capsule defect displayed a defect in the mammalian host, using a murine inhalation model. We infected mice with a mixture of differentially-tagged wild-type and mutant cells at a ratio of 1:1. At 10 days post infection (dpi), we sacrificed animals, harvested and homogenized lung tissue, then plated on the appropriate selective media for colony forming units (CFUs). All but one of the *pbx1* /*cpl1* cluster members were significantly underrepresented relative to wild-type; the exception was the *cnag\_01058* mutant, which is defective in capsule maintenance but not capsule biosynthesis (Fig. 4C, S4A). *yap1* cells, which appear acapsular but secrete GXM, displayed a major defect in fitness in the host (Fig. 4E). Three of four *cap60* cluster mutants also display a defect in accumulation of CFUs in host lungs (Fig. 4E).

### Chemogenomics identifies the cell cycle as a target of the anti-fungal small molecule S8

We included a number of drug-like antifungal compounds in our screen in order to identify their targets (Table 1). Our use of *C. neoformans* chemogenomics to assist in the identification of a target of toremifene is described elsewhere (Butts *et al.*, 2014). Here we investigate the thiazolidine-2,4-dione derivatives originally described for their activity against *C. albicans* biofilms (Kagan *et al.*, 2013).

Our chemogenomic profiling data of the thiazolidine-2,4-dione derivative S8 revealed a striking outlier: a knockout mutant in the gene coding for a *C. neoformans* ortholog of the conserved cell cycle kinase Wee1, is relatively resistant (Fig. 5A). We observed resistance at multiple concentrations of S8 (Table S2). The related compound NA8, which contains a replacement of a sulfur atom with a carbon atom on the thiazolidinedione moiety (Fig. 5B), does not elicit the same resistance (Fig. S3A). The *wee1* mutant is also resistant to S10 (Fig. S3B), which harbors a C10 alkyl chain instead of C8 but is otherwise identical to S8 (Fig. S3C).

Wee1 regulates the G2/M cell cycle checkpoint through inhibitory phosphorylation of Cdk1, which in turn is required for cells to traverse the checkpoint. The essential phosphatase



Cdc25 activates Cdk1 by removing the inhibitory phosphorylation added by Wee1 (Morgan, 2007) (Fig. 5C). Because the *wee1* is relatively resistant to S8, we hypothesized that S8 targeted a protein that acts through Wee1 to regulate Cdk1. One such target could be Cdc25.

We reasoned that if the Wee1/Cdc25-regulated step of the cell cycle were an important target of S8 *in vivo*, wild-type *C. neoformans* cells treated with S8 would arrest at G2/M. To test this prediction, we treated exponential cultures with S8, S10, or NA8 and examined the impact on the cell cycle. We harvested and fixed representative samples every 30 minutes, then analyzed DNA content by flow cytometry. Control cultures treated with DMSO (carrier) (Fig. 5D) or the control compound NA8 (Fig. 5E) stayed asynchronous for the entire 3.5 hrs of the time course. Strikingly, S8-treated (Fig. 5F) cells accumulated with 2C DNA content, which indicates G2/M arrest in *C. neoformans*, a haploid yeast (Whelan and Kwon-Chung, 1986). At later timepoints, cells synthesize DNA but do not complete mitosis and cytokinesis. This is consistent with observations in *S. pombe* that partial inhibition of Cdk1 permits re-replication of DNA (Broek *et al.*, 1991).

Because inhibition of Cdc25 would provide a parsimonious explanation for the genetic and biological properties of S8, we tested whether S8 inhibits *C. neoformans* Cdc25 *in vitro*. We expressed and purified the catalytic domain of a *C. neoformans* ortholog (*CNAG\_07942*) in *E. coli* (Fig. S3D) and then performed *in vitro* phosphatase assays using 3-O-methyl fluorescein phosphate (OMFP) as a substrate (Fig. 5G, H) (Hill *et al.*, 1968). We observed that S8 inhibits Cdc25 activity ( $K_i \sim 140\mu\text{M}$ , Fig. 5E), as do both S10 (Fig. S3E) and NSC 663284 ( $K_i \sim 250\mu\text{M}$ , Fig. S3F), a commercially available inhibitor of mammalian Cdc25 (Pu *et al.*, 2002). The control compound NA8 does not inhibit *C. neoformans* Cdc25 *in vitro* (Fig. S3G). For S8, the *in vitro* inhibition constant is roughly comparable to the liquid MIC value against *C. neoformans*, which we measured to be  $\sim 60\mu\text{M}$  in YNB. S10 has a higher  $K_i$  ( $K_i \sim 310\mu\text{M}$ ) but similar to the MIC value ( $\sim 55\mu\text{M}$ ) measured in YNB agar compared to S8.

## O2M: a genetic biomarker algorithm to predict compound synergies

Drug resistance is a major clinical challenge in the treatment of both bacterial and fungal infections (Anderson, 2005; Cantas *et al.*, 2013). An effective therapeutic strategy is to treat patients with drugs that act synergistically, enhancing each other's effectiveness beyond that produced by the sum of each drug's individual impact (Kalan and Wright, 2011). This approach is thought to decrease acquisition drug resistance, increase the available drug repertoire (Kalan and Wright, 2011) and ameliorate toxicities (Kathiravan *et al.*, 2012; Lehar *et al.*, 2009).

We hypothesized that we could use the chemogenomic information from our screens of drugs known to act synergistically, such as FLC and fenpropimorph (Jansen *et al.*, 2009) to identify new synergistic interactions (Fig. 6A). When we compared the identity of genes whose knockouts "responded" to each individual small molecule in a known synergistic pair ( $|Z| \geq 2.5$ , Table S3–S4), we found that this "responsive" gene set was significantly enriched over the expected value (Fisher's exact test,  $p = 6 \times 10^{-5}$ ) (Fig. 6A, top). This observation is consistent with a previous report that the chemical-genetic response to each drug in a synergistic pair is enriched for overlapping genes (Jansen *et al.*, 2009).

This overlap in responsive gene sets led us to consider the possibility that overlapping responsive genes from known synergistic compound pairs could be used as biomarkers to predict new synergistic combinations. Our method involves first identifying the overlaps in responsive gene sets for all compounds that had been reported in the literature to synergize with a small molecule of interest (“compound X”), selecting those genes common to all of those sets (Fig. 6A, middle – the overlaps of overlaps). We refer to these genes as “synergy biomarker genes.” Critically, we next hypothesized that any compound that contains one or more of these synergy biomarker genes in its responsive gene set would be synergistic with compound X. Because our method used the overlaps of response gene overlaps between compounds known to be synergistic, we refer to it as the “overlap-squared method” or “O2M.”

We then tested O2M using two drugs for which substantial literature synergy information was available: FLC and geldanamycin (GdA). FLC is an approved antifungal drug. GdA is an inhibitor of Hsp90, a chaperone protein with many physical and genetic interactions (Taipale *et al.*, 2010). We performed our analysis on fenpropimorph and sertraline, which are known to act synergistically with FLC (Jansen *et al.*, 2009; Zhai *et al.*, 2012) and cyclosporine and rapamycin, which are known to act synergistically with GdA (Francis *et al.*, 2006; Kumar *et al.*, 2005). Using this prior knowledge and our data, we identified synergy biomarker genes for FLC (*CNAG\_00573*, *CNAG\_03664*, and *CNAG\_03917*) and GdA (*CNAG\_01172*, *CNAG\_03829*, and *CNAG\_01862*). We generated a list of compounds from our chemical-genetics dataset that contain one or more of these genes in their responsive genes set.

We then used a standard “checkerboard” assay to experimentally determine fractional inhibitory concentration index (FICI), and we adopted the standard that an FICI value below 0.5 is synergistic (Meletiadiis *et al.*, 2010). We determined FICIs for FLC and GdA with three sets of compounds: 1) the compounds predicted from synergy biomarker genes, 2) the predicted synergistic compounds for the other drug (e.g. we tested compounds predicted to be synergistic with GdA for synergy with FLC), and 3) a randomly generated subset of the compounds not predicted to act synergistically with either FLC or GdA. The second and third groups are as controls for compounds that are generally synergistic and to determine the background frequency of synergistic interactions within a set of compounds.

Respective experimental FICI values for FLC and GdA are shown in Fig. 6B and 6C (yellow bars: synergy; blue bars additive or worse interactions). The labels for compounds we predicted to be synergistic are colored purple, positive controls (published synergistic compound pairs) are colored green, and predicted negative control compounds colored blue (Fig. 6). We observed that only ~10% of the negative control compounds act synergistically with either FLC or GdA. In striking contrast, we found ~80% and ~60% of the compounds selected by O2M are synergistic with FLC and GdA, respectively. Thus, for two unrelated compounds, O2M is highly successful at predicting synergistic interactions and performs vastly better than the brute force trial-and-error approach (Fig. 6D, E) ( $p < 0.0008$ , Fisher’s exact test).

## Discussion

We applied chemogenomic profiling to the major fungal driver of AIDS-related death, the encapsulated yeast *C. neoformans*, to produce a chemical-genetic atlas of this important pathogen. Beyond identifying new virulence factors and compound mode-of-action, we describe a conceptually general approach to identifying drug synergies that combines prior knowledge and chemogenomic profiles to identify compound synergies.

### A chemical-genetic atlas for *Cryptococcus neoformans*

We maximized the quality of the atlas in several ways. To capture concentration-dependent impacts of compounds, we obtained MIC for each compound and examined the genetic responses at multiple concentrations below MIC. In addition, we performed a large number of control screens and incorporated batch information for systematic correction. Overall benchmarks of data quality (Fig. 1) together with nearest neighbor and Gene Ontology analysis (Fig. 2) support the existence of substantial chemical-genetic signal in the data. Even genes with orthologs in both *S. cerevisiae* and *C. neoformans* show considerable differences in responses (Fig. 3). While this may not be surprising given the large phylogenetic distance between these fungi, it shows that understanding the chemical responses of pathogens requires pathogen-focused studies, even when considering conserved genes and processes. For example, we observed differences in the responses to azole drugs between *S. cerevisiae* and *C. neoformans* (Fig. 3). Since azoles are heavily used clinically, differences in responses between species are of significant interest.

### Insights gained from initial use of the *C. neoformans* chemical-genetic atlas

**Identification of mutants that impact capsule formation and mammalian infection**—Our studies on capsule biosynthesis genes focused two different clusters that contained genes that we and others have shown to be required for capsule formation, the *pbx1/cpl1* cluster and the *cap60* cluster. As anticipated from model organism studies (Collins *et al.*, 2007; Costanzo *et al.*, 2010; Nichols *et al.*, 2010; Parsons *et al.*, 2004; Parsons *et al.*, 2006), these clusters were indeed enriched for genes whose mutants are defective in capsule biosynthesis and mammalian pathogenesis. The genes represented by the two clusters differed functionally in that genes in the *pbx1/cpl1* cluster but not the *cap60* cluster are required for association of capsule polysaccharide with the cell surface (Fig. 4, S4). A recent study on Pbx1 and its ortholog, Pbx2, proposes that the two proteins act redundantly in capsule assembly (Kumar *et al.*, 2014). *pbx1* and *pbx2* cells shed lower amounts of GXM into the culture medium but that the GXM functions in a capsule transfer assay. Electron microscopy studies indicate that these mutants exhibit defects in the cell wall. Our data are fully consistent with these data. Other genes from the *pbx1/cpl1* cluster likely play a role in these processes. Some, like *GCN5* and *SGF73*, which encode orthologs of the yeast SAGA histone acetylase/deubiquitylase complex, are clearly regulatory, while others could act more directly. While detailed validation and investigation of these many candidates (including gene deletion reconstruction studies) will be required to obtain mechanistic insight into capsule biology, their enrichment suggests value of this *Cryptococcal* chemogenomic resource in identifying mutants defective in virulence.

**Compound target identification**—Chemogenomic profiling has proven useful in identifying targets of uncharacterized compounds (Parsons *et al.*, 2006), including in the pathogenic fungus *C. albicans* (Jiang *et al.*, 2008; Xu *et al.*, 2007; Xu *et al.*, 2009). Chemical-genetic data can be used to determine the target of compounds within complex mixtures (Jiang *et al.*, 2008; Xu *et al.*, 2009). Our goal differed: we sought to identify targets of repurposed compounds, as described elsewhere (Butts *et al.*, 2013), or, in the case of S8, a compound identified as an inhibitor of *Candida* biofilms (Kagan *et al.*, 2013). The identification of the Wee1 kinase as a sensitivity determinant for S8, the cell cycle arrest produced by S8, and the ability of the compound to inhibit *Cn*Cdc25 *in vitro* together support the model that S8 inhibits growth through via the cell cycle at least in part via inhibition of Cdc25. Whether this explains its impact on biofilms requires further investigation. As with any compound target, ultimate proof that Cdc25 is the target of S8 will require the isolation of resistance alleles of *CDC25*.

Given the simplicity of the pharmacophore and its  $K_i$  for *Cn*Cdc25, it would not be surprising if S8 had additional cellular targets, as recently described (Feldman *et al.*, 2014). Cdc25 is a conserved cell cycle phosphatase and therefore might be considered a poor drug target *a priori* but cyclin-dependent kinases are a focus of recent anti-parasite therapeutics (Geyer *et al.*, 2005). It is also notable that the target of azole antifungals, lanosterol 14-demethylase (Ghannoum and Rice, 1999) is conserved from yeast to human.

**O2M: predicting compound synergies using prior knowledge and chemical profiles**—Identifying synergistic drug interactions is of considerable clinical interest, but efficient methods for their identification are elusive. Systematic examination of combinations of a small set of compounds using *S. cerevisiae* suggests that synergies are relatively rare and often involve so-called “promiscuous” synergizers, compounds that are synergistic with multiple partners (Cokol *et al.*, 2011). Chemogenomic studies have shown that drugs known to be synergistic tend to have overlapping “responding” gene sets (Jansen *et al.*, 2009). We expanded on this concept to develop a highly parallel method, O2M, for efficiently predicting synergistic drug interactions. Our work utilizes prior knowledge of drug synergies to identify a discrete set of predictive biomarker genes for a given compound. We experimentally demonstrated the utility of O2M for two compounds, FLC and geldanamycin. Our method identified dozens of synergistic interactions and discovered a small number of biomarkers that could serve as readouts for further screens for synergistic drugs. The method appears to not simply select promiscuous synergizers: five of six drugs previously classified as promiscuous synergizers (Cokol *et al.*, 2011) were tested in our studies but most were not predicted to be synergistic by O2M. One of the promiscuous compounds was a positive control (fenpropimorph with FLC) and another (dyclonine) was predicted synergistic with FLC but was not and was predicted not synergistic with GdA but was. We anticipate that O2M could be used to identify synergistic compound interactions in published *E. coli* and *C. albicans* chemical-genetics datasets (Jiang *et al.*, 2008; Nichols *et al.*, 2010; Xu *et al.*, 2007; Xu *et al.*, 2009).

## Experimental Procedures

### Determination of MICs

We determined minimum inhibitory concentration (MIC) on solid growth medium for each compound used in screening (Table 1).

### Colony array-based chemogenomic profiling

*C. neoformans* knockouts were inoculated from frozen 384-well plates to YNB + 2% glucose. Plates were grown 24hrs at 30°C, then used to inoculate screening plates containing compounds of interest.

### Data analysis

Data were analyzed as previously described (Baryshnikova *et al.*, 2010) with the a few exceptions.

### *C. neoformans* ortholog identification and GO term mapping

Mapping from *S. cerevisiae* Uniprot Proteins to *C. neoformans* Uniprot Proteins was done using One-to-one mappings in MetaPhOrs (<http://metaphors.phylomedb.org/>). *C. neoformans* ORFs were compared to a database of *S. cerevisiae* Uniprot Proteins using blastp (Altschul *et al.*, 1997) with a E-score cutoff of  $10^{-30}$ . Corresponding yeast GO annotations were mapped onto the *C. neoformans* ORFs.

### Comparison of transcriptional response to FLC

Compared transcriptional responses between *S. cerevisiae* (Kuo *et al.*, 2010) and *C. neoformans* (Florio *et al.*, 2011).

### Capsule induction assay

Samples were grown overnight at 30°C in 100% Sabouraud's broth, then diluted 1:100 into 10% Sabouraud's broth buffered with 50mM HEPES pH 7.3 and grown for 3 days at 37°C. India ink was added at 3:1 ratio and samples imaged on a Zeiss Axiovert microscope.

### Capsule transfer assay

Performed as in (Reese and Doering, 2003), with minor modifications.

### GXM immunoblot assay

Conditioned medium was made from donor GXM donor strains as described above.

### Mouse infection assay

Mouse lung infections were performed as previously described (Chun *et al.*, 2011).

### Cdc25 protein purification

We identified the *C. neoformans* ortholog of Cdc25, *CNAG\_01572*, by best reciprocal BLAST (Altschul *et al.*, 1997) hit with the human Cdc25A, Cdc25B, and Cdc25C protein

isoforms. We then inserted the exonic sequence of the catalytic domain into a 6x-His tag expression vector for purification.

### Cdc25 phosphatase assay

Cdc25 phosphatase activity was analyzed in activity buffer (50mM Tris pH 8.3, 5% glycerol, 0.8mM dithiothreitol, and 1% PVA).

### Cdc25 inhibitor treatment and FACS analysis

Wild-type *C. neoformans* was grown overnight in 1x YNB at 30°C with rotation. Cultures were diluted to OD<sub>600</sub> ~ 0.2 into 150ml 1x YNB, then incubated 3hr at 30°C. Samples were then split and NA8, S8, and S10 added to 60μM. Equivalent volume of DMSO was added to the control culture.

### Fractional Inhibitory Concentration Index (FICI) assay for synergy

We determined FICI using a standard checkerboard assay (Hsieh *et al.*, 1993), calculating FICI as described using a 50% growth inhibition cutoff for MICs for individual compounds (Hsieh *et al.*, 1993; Meletiadis *et al.*, 2010), then using a standard cutoff of FICI < 0.5 to define synergy.

See Extended Experimental Procedures for additional details.

## Supplementary Material

Refer to Web version on PubMed Central for supplementary material.

## Acknowledgments

This work was supported by NIH grants 5R01AI099206 to H.D.M., 1R01AI091422 to D.J.K., 1R01HG005084 and 1R01GM04975 to C.L.M., and a grant from the CIFAR Genetic Networks Program to C.L.M.

## References

- Altschul SF, Madden TL, Schaeffer AA, Zhang J, Zhang Z, Miller W, Lipman DJ. Gapped BLAST and PSI-BLAST: a new generation of protein database search programs. *Nucleic Acids Res.* 1997; 25:3389–3402. [PubMed: 9254694]
- Anderson JB. Evolution of antifungal-drug resistance: mechanisms and pathogen fitness. *Nature Reviews Microbiology.* 2005; 3:547–556.
- Armstrong-James D, Meintjes G, Brown GD. A neglected epidemic: fungal infections in HIV/AIDS. *Trends Microbiol.* 2014; 22:120–127. [PubMed: 24530175]
- Baryshnikova A, Costanzo M, Kim Y, Ding H, Koh J, Toufighi K, Youn JY, Ou J, San Luis BJ, Bandyopadhyay S, et al. Quantitative analysis of fitness and genetic interactions in yeast on a genome scale. *Nat Meth.* 2010; 7:1017–1024.
- Broek D, Bartlett R, Crawford K, Nurse P. Involvement of p34cdc2 in establishing the dependency of S phase on mitosis. *Nature.* 1991; 349:388–393. [PubMed: 1992340]
- Butts A, DiDone L, Koselny K, Baxter BK, Chabrier-Rosello Y, Wellington M, Krysan DJ. A Repurposing Approach Identifies Off-Patent Drugs with Fungicidal Cryptococcal Activity, a Common Structural Chemotype, and Pharmacological Properties Relevant to the Treatment of Cryptococcosis. *Eukaryot Cell.* 2013; 12:278–287. [PubMed: 23243064]

- Butts A, Koselny K, Chabrier-Roselló Y, Semighini CP, Brown JCS, Wang X, Annadurai S, DiDone L, Tabroff J, Childers WE, et al. Estrogen Receptor Antagonists Are Anti-Cryptococcal Agents That Directly Bind EF Hand Proteins and Synergize with Fluconazole In Vivo. *mBio*. 2014;5.
- Butts A, Krysan DJ. Antifungal Drug Discovery: Something Old and Something New. *PLoS Pathog*. 2012; 8:e1002870. [PubMed: 22969422]
- Cantas L, Shah SQA, Cavaco LM, Manaia C, Walsh F, Popowska M, Garelick H, Bürgmann H, Sørum H. A brief multi-disciplinary review on antimicrobial resistance in medicine and its linkage to the global environmental microbiota. *Front Microbiol*. 2013; 4:96. [PubMed: 23675371]
- Chang YC, Kwon-Chung KJ. Isolation of the Third Capsule-Associated Gene, CAP60, Required for Virulence in *Cryptococcus neoformans*. *Infect Immun*. 1998; 66:2230–2236. [PubMed: 9573112]
- Chun CD, Brown JCS, Madhani HD. A Major Role for Capsule-Independent Phagocytosis-Inhibitory Mechanisms in Mammalian Infection by *Cryptococcus neoformans*. *Cell Host Microbe*. 2011; 9:243–251. [PubMed: 21402362]
- Cokol M, Chua HN, Tasan M, Mutlu B, Weinstein ZB, Suzuki Y, Nergiz ME, Costanzo M, Baryshnikova A, Giaever G, et al. Systematic exploration of synergistic drug pairs. *Mol Syst Biol*. 2011; 7:544. [PubMed: 22068327]
- Collins SR, Miller KM, Maas NL, Roguev A, Fillingham J, Chu CS, Schuldiner M, Gebbia M, Recht J, Shales M, et al. Functional dissection of protein complexes involved in yeast chromosome biology using a genetic interaction map. *Nature*. 2007; 446:806–810. [PubMed: 17314980]
- Costanzo M, Baryshnikova A, Bellay J, Kim Y, Spear ED, Sevier CS, Ding H, Koh JLY, Toufighi K, Mostafavi S, et al. The Genetic Landscape of a Cell. *Science*. 2010; 327:425–431. [PubMed: 20093466]
- Del Poeta M. Role of phagocytosis in the virulence of *Cryptococcus neoformans*. *Eukaryot Cell*. 2004; 3:1067–1075. [PubMed: 15470235]
- Dittmar J, Reid R, Rothstein R. ScreenMill: A freely available software suite for growth measurement, analysis and visualization of high-throughput screen data. *BMC Bioinformatics*. 2010; 11:353–363. [PubMed: 20584323]
- Doering TL. How sweet it is! Cell wall biogenesis and polysaccharide capsule formation in *Cryptococcus neoformans*. *Annu Rev Microbiol*. 2009; 63:223–247. [PubMed: 19575556]
- Feldman M, Al-Quntar A, Polacheck I, Friedman M, Steinberg D. Therapeutic Potential of Thiazolidinedione-8 as an Antibiofilm Agent against *Candida albicans*. *PLoS One*. 2014; 9:e93225. [PubMed: 24796422]
- Fernández L, Hancock REW. Adaptive and Mutational Resistance: Role of Porins and Efflux Pumps in Drug Resistance. *Clin Microbiol Rev*. 2012; 25:661–681. [PubMed: 23034325]
- Florio A, Ferrari S, De Carolis E, Torelli R, Fadda G, Sanguinetti M, Sanglard D, Posteraro B. Genome-wide expression profiling of the response to short-term exposure to fluconazole in *Cryptococcus neoformans* serotype A. *BMC Microbiol*. 2011; 11:97. [PubMed: 21569340]
- Francis LK, Alsayed Y, Leleu X, Jia X, Singha UK, Anderson J, Timm M, Ngo H, Lu G, Huston A, et al. Combination Mammalian Target of Rapamycin Inhibitor Rapamycin and HSP90 Inhibitor 17-Allylamino-17-Demethoxygeldanamycin Has Synergistic Activity in Multiple Myeloma. *Clinical Cancer Research*. 2006; 12:6826–6835. [PubMed: 17121904]
- Geyer JA, Prigge ST, Waters NC. Targeting malaria with specific CDK inhibitors. *Biochim Biophys Acta*. 2005; 1754:160–170. [PubMed: 16185941]
- Ghannoum MA, Rice LB. Antifungal agents: mode of action, mechanisms of resistance, and correlation of these mechanisms with bacterial resistance. *Clin Microbiol Rev*. 1999; 12:501–517. [PubMed: 10515900]
- Haynes BC, Skowrya ML, Spencer SJ, Gish SR, Williams M, Held EP, Brent MR, Doering TL. Toward an integrated model of capsule regulation in *Cryptococcus neoformans*. *PLoS Pathog*. 2011; 7:e1002411. [PubMed: 22174677]
- Heitman, J.; Kozel, TR.; Kwon-Chung, KJ.; Perfect, JR.; Casadevall, A., editors. *Cryptococcus: from human pathogen to model yeast*. Washington, D.C: ASM Press; 2011.
- Hill HD, Summer GK, Waters MD. An automated fluorometric assay for alkaline phosphatase using 3-O-methylfluorescein phosphate. *Analytical Biochemistry*. 1968; 24:9–17. [PubMed: 5665203]

- Hillenmeyer ME, Fung E, Wildenhain J, Pierce SE, Hoon S, Lee W, Proctor M, St Onge RP, Tyers M, Koller D, et al. The Chemical Genomic Portrait of Yeast: Uncovering a Phenotype for All Genes. *Science*. 2008; 320:362–365. [PubMed: 18420932]
- Hsieh MJ, Yu CM, Yu VL, Chow JW. Synergy assessed by checkerboard: a critical analysis. *Diagnostic Microbiology and Infectious Disease*. 1993; 16:343–349. [PubMed: 8495592]
- Janbon G, Ormerod KL, Paulet D, Byrnes EJ III, Yadav V, Chatterjee G, Mullapudi N, Hon C-C, Billmyre RB, Brunel F, et al. Analysis of the Genome and Transcriptome of *Cryptococcus neoformans* var. *grubii* Reveals Complex RNA Expression and Microevolution Leading to Virulence Attenuation. *PLoS Genet*. 2014; 10:e1004261. [PubMed: 24743168]
- Jansen G, Lee AY, Epp E, Fredette A, Surprenant J, Harcus D, Scott M, Tan E, Nishimura T, Whiteway M, et al. Chemogenomic profiling predicts antifungal synergies. *Mol Syst Biol*. 2009;5.
- Jiang B, Xu D, Allocco J, Parish C, Davison J, Veillette K, Sillaots S, Hu W, Rodriguez-Suarez R, Trosok S, et al. PAP Inhibitor with In Vivo Efficacy Identified by *Candida albicans* Genetic Profiling of Natural Products. *Chem Biol*. 2008; 15:363–374. [PubMed: 18420143]
- Kagan S, Jabbour A, Sionov E, Alquntar AA, Steinberg D, Srebnik M, Nir-Paz R, Weiss A, Polacheck I. Anti-*Candida albicans* biofilm effect of novel heterocyclic compounds. *J Antimicrob Chemother*. 2013;68. [PubMed: 23011289]
- Kalan L, Wright GD. Antibiotic adjuvants: multicomponent anti-infective strategies. *Expert Rev Mol Med*. 2011; 13:null–null.
- Kathiravan MK, Salake AB, Chothe AS, Dudhe PB, Watode RP, Mukta MS, Gadhw S. The biology and chemistry of antifungal agents: A review. *Bioorganic & Medicinal Chemistry*. 2012; 20:5678–5698. [PubMed: 22902032]
- Kozel TR, Hermerath CA. Binding of cryptococcal polysaccharide to *Cryptococcus neoformans*. *Infect Immun*. 1984; 43:879–886. [PubMed: 6365785]
- Kozel TR, Levitz SM, Dromer F, Gates MA, Thorkildson P, Janbon G. Antigenic and Biological Characteristics of Mutant Strains of *Cryptococcus neoformans* Lacking Capsular O Acetylation or Xylosyl Side Chains. *Infect Immun*. 2003; 71:2868–2875. [PubMed: 12704160]
- Kumar P, Heiss C, Santiago-Tirado FH, Black I, Azadi P, Doering TL. Pbx proteins in *Cryptococcus neoformans* cell wall remodeling and capsule assembly. *Eukaryot Cell*. 2014
- Kumar P, Yang M, Haynes BC, Skowrya ML, Doering TL. Emerging themes in cryptococcal capsule synthesis. *Current Opinion in Structural Biology*. 2011; 21:597–602. [PubMed: 21889889]
- Kumar R, Musiyenko A, Barik S. Plasmodium falciparum calcineurin and its association with heat shock protein 90: mechanisms for the antimalarial activity of cyclosporin A and synergism with geldanamycin. *Mol Biochem Parasitol*. 2005; 141:29–37. [PubMed: 15811524]
- Kuo D, Tan K, Zinman G, Ravasi T, Bar-Joseph Z, Ideker T. Evolutionary divergence in the fungal response to fluconazole revealed by soft clustering. *Genome Biol*. 2010; 11:R77. [PubMed: 20653936]
- Lehar J, Krueger AS, Avery W, Heilbut AM, Johansen LM, Price ER, Rickles RJ, Short GF III, Staunton JE, Jin X, et al. Synergistic drug combinations tend to improve therapeutically relevant selectivity. *Nat Biotechnol*. 2009; 27:659–666. [PubMed: 19581876]
- Liu C, Apodaca J, Davis LE, Rao H. Proteasome inhibition in wild-type yeast *Saccharomyces cerevisiae* cells. *Biotechniques*. 2007a; 42:158–162. [PubMed: 17373478]
- Liu OW, Chun CD, Chow ED, Chen C, Madhani HD, Noble SM. Systematic Genetic Analysis of Virulence in the Human Fungal Pathogen *Cryptococcus neoformans*. *Cell*. 2008; 135:174–188. [PubMed: 18854164]
- Liu OW, Kelly MJS, Chow ED, Madhani HD. Parallel  $\beta$ -Helix Proteins Required for Accurate Capsule Polysaccharide Synthesis and Virulence in the Yeast *Cryptococcus neoformans*. *Eukaryot Cell*. 2007b; 6:630–640. [PubMed: 17337638]
- Loyse A, Bicanic T, Jarvis JN. Combination Antifungal Therapy for Cryptococcal Meningitis. *N Engl J Med*. 2013; 368:2522–2523. [PubMed: 23802522]
- Lozano R, Naghavi M, Foreman K, Lim S, Shibuya K, Aboyans V, Abraham J, Adair T, Aggarwal R, Ahn SY, et al. Global and regional mortality from 235 causes of death for 20 age groups in 1990 and 2010: a systematic analysis for the Global Burden of Disease Study 2010. *Lancet*. 2012; 380:2095–2128. [PubMed: 23245604]



- Mandell, GL.; Bennett, JE.; Dolin, R. Mandell, Douglas, and Bennett's Principles and Practice of Infectious Diseases. 7. Philadelphia: Churchill Livingstone Elsevier; 2010.
- Meletiadiis J, Pournaras S, Roilides E, Walsh TJ. Defining fractional inhibitory concentration index cutoffs for additive interactions based on self-drug additive combinations, Monte Carlo simulation analysis, and *in vitro-in vivo* correlation data for antifungal drug combinations against *Aspergillus fumigatus*. *Antimicrob Agents Chemother.* 2010; 54:602–609. [PubMed: 19995928]
- Morgan, DO. The Cell Cycle: Principles of Control. London, UK: New Science Press; 2007.
- Nichols RJ, Sen S, Choo YJ, Beltrao P, Zietek M, Chaba R, Lee S, Kazmierczak KM, Lee KJ, Wong A, et al. Phenotypic Landscape of a Bacterial Cell. *Cell.* 2010; 144:143–156. [PubMed: 21185072]
- O'Meara TR, Alspaugh JA. The *Cryptococcus neoformans* Capsule: a Sword and a Shield. *Clin Microbiol Rev.* 2012; 25:387–408. [PubMed: 22763631]
- O'Meara TR, Norton D, Price MS, Hay C, Clements MF, Nichols CB, Alspaugh JA. Interaction of *Cryptococcus neoformans* Rim101 and protein kinase A regulates capsule. *PLoS Pathog.* 2010; 6:e1000776. [PubMed: 20174553]
- Park BJ, Wannemuehler KA, Marston BJ, Govender N, Pappas PG, Chiller TM. Estimation of the current global burden of cryptococcal meningitis among persons living with HIV/AIDS. *AIDS.* 2009; 23:525–530. [PubMed: 19182676]
- Parsons AB, Brost RL, Ding H, Li Z, Zhang C, Sheikh B, Brown GW, Kane PM, Hughes TR, Boone C. Integration of chemical-genetic and genetic interaction data links bioactive compounds to cellular target pathways. *Nat Biotech.* 2004; 22:62–69.
- Parsons AB, Lopez A, Givoni IE, Williams DE, Gray CA, Porter J, Chua G, Sopko R, Brost RL, Ho CH, et al. Exploring the Mode-of-Action of Bioactive Compounds by Chemical-Genetic Profiling in Yeast. *Cell.* 2006; 126:611–625. [PubMed: 16901791]
- Pu L, Amoscato AA, Bier ME, Lazo JS. Dual G1 and G2 Phase Inhibition by a Novel, Selective Cdc25 Inhibitor 7-Chloro-6-(2-morpholin-4-ylethylamino)- quinoline-5,8-dione. *J Biol Chem.* 2002; 277:46877–46885. [PubMed: 12356752]
- Reese AJ, Doering TL. Cell wall  $\alpha$ -1,3-glucan is required to anchor the *Cryptococcus neoformans* capsule. *Mol Microbiol.* 2003; 50:1401–1409. [PubMed: 14622425]
- Roemer T, Xu D, Singh Sheo B, Parish Craig A, Harris G, Wang H, Davies Julian E, Bills Gerald F. Confronting the Challenges of Natural Product-Based Antifungal Discovery. *Chem Biol.* 2011; 18:148–164. [PubMed: 21338914]
- Taipale M, Jarosz DF, Lindquist S. HSP90 at the hub of protein homeostasis: emerging mechanistic insights. *Nature Reviews Molecular Cellular Biology.* 2010; 11:515–528.
- Vecchiarelli A, Pericolini E, Gabrielli E, Kenno S, Perito S, Cenci E, Monari C. Elucidating the immunological function of the *Cryptococcus neoformans* capsule. *Future Microbiol.* 2013; 8:1107–1116. [PubMed: 24020739]
- Whelan WL, Kwon-Chung KJ. Genetic complementation in *Cryptococcus neoformans*. *J Bacteriol.* 1986; 166:924–929. [PubMed: 3519586]
- WHO. W.H.O. Library. Rapid Advice: diagnosis, prevention and management of cryptococcal disease in HIV-infected adults, adolescents, and children. Geneva, Switzerland: WHO Press; 2011.
- Xu D, Jiang B, Ketela T, Lemieux S, Veillette K, Martel N, Davison J, Sillaots S, Trosok S, Bachewich C, et al. Genome-Wide Fitness Test and Mechanism-of-Action Studies of Inhibitory Compounds in *Candida albicans*. *PLoS Pathog.* 2007; 3:e92. [PubMed: 17604452]
- Xu D, Sillaots S, Davison J, Hu W, Jiang B, Kauffman S, Martel N, Ocampo P, Oh C, Trosok S, et al. Chemical Genetic Profiling and Characterization of Small-molecule Compounds That Affect the Biosynthesis of Unsaturated Fatty Acids in *Candida albicans*. *J Biol Chem.* 2009; 284:19754–19764. [PubMed: 19487691]
- Zhai B, Wu C, Wang L, Sachs MS, Lin X. The Antidepressant Sertraline Provides a Promising Therapeutic Option for Neurotropic Cryptococcal Infections. *Antimicrob Agents Chemother.* 2012; 56:3758–3766. [PubMed: 22508310]

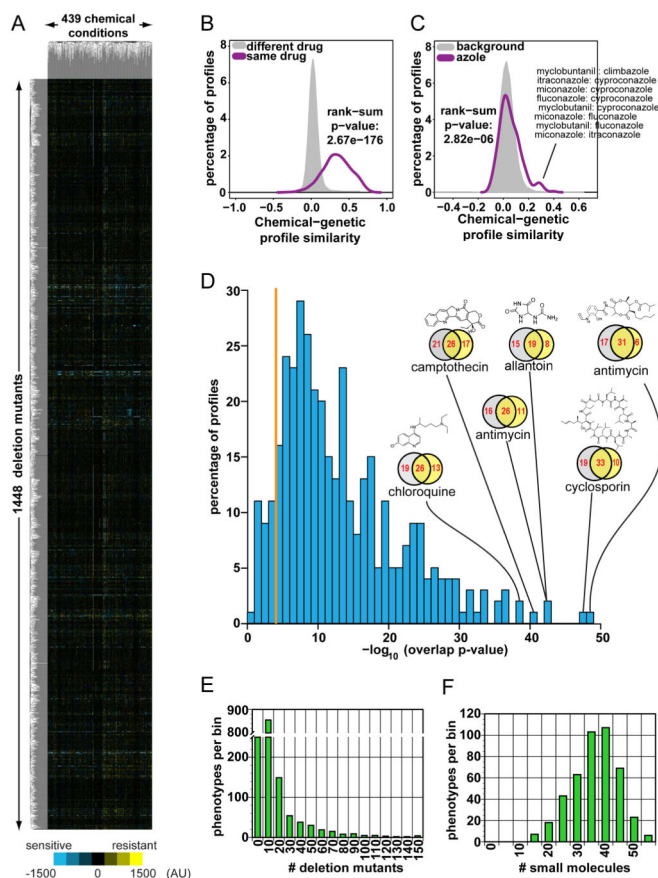


**Figure 1. Chemical-genetic profiling of *C. neoformans***

A) Heat map of full dataset following hierarchical clustering. Compounds are arrayed on the x-axis and gene knockouts on the y-axis. See also Tables S1–S2.

B) Probability density function for pairwise correlation scores between the chemical genetic profiles of different compounds (grey) and the same compounds at different concentrations (purple) screened on different days (different batches). Scores between the chemical-genetic profiles of different concentrations of the same compounds are significantly higher than those between different compounds (Wilcoxon test,  $p = 2.7 \times 10^{-176}$ ). See also Fig. S1.

C) Probability density function for pairwise correlation scores between the chemical genetic profiles of different compounds (grey) and azole family compounds (purple). Pairwise comparisons between azoles exhibit higher correlation scores than non-azole compounds (Wilcoxon test,  $p = 2.8 \times 10^{-6}$ ). Molecules with the highest pairwise comparisons scores are listed on the right.

D) Pearson's correlation score between two different concentrations of the same compounds. Concentrations with similar correlation scores are binned together (y-axis). For compounds with the greatest correlation scores between concentrations, Venn diagrams of significant genes ( $Z < -2.5$ ) present in profiles from the same compounds at different concentrations and the small molecule structure are shown. The orange line indicates a hypergeometric p-value 0.05

E) Distribution of the number of significant phenotypes for each knockout mutant. Significant is considered  $|Z| > 2.5$  and we identified significant phenotypes independently

for each small molecule concentration. Knockout mutants with similar numbers of significant phenotypes are binned together (x-axis).

F) Distribution of the number of significant phenotypes ( $|Z| > 2.5$ ) for each small molecule condition/concentration. Molecules with similar numbers of significant phenotypes were binned together (x-axis) and the # phenotypes per bin is shown on the y-axis. Bin range on the x-axis is 0, 1–5, 6–10, etc.

See also Fig. S1 and Tables S1–5.

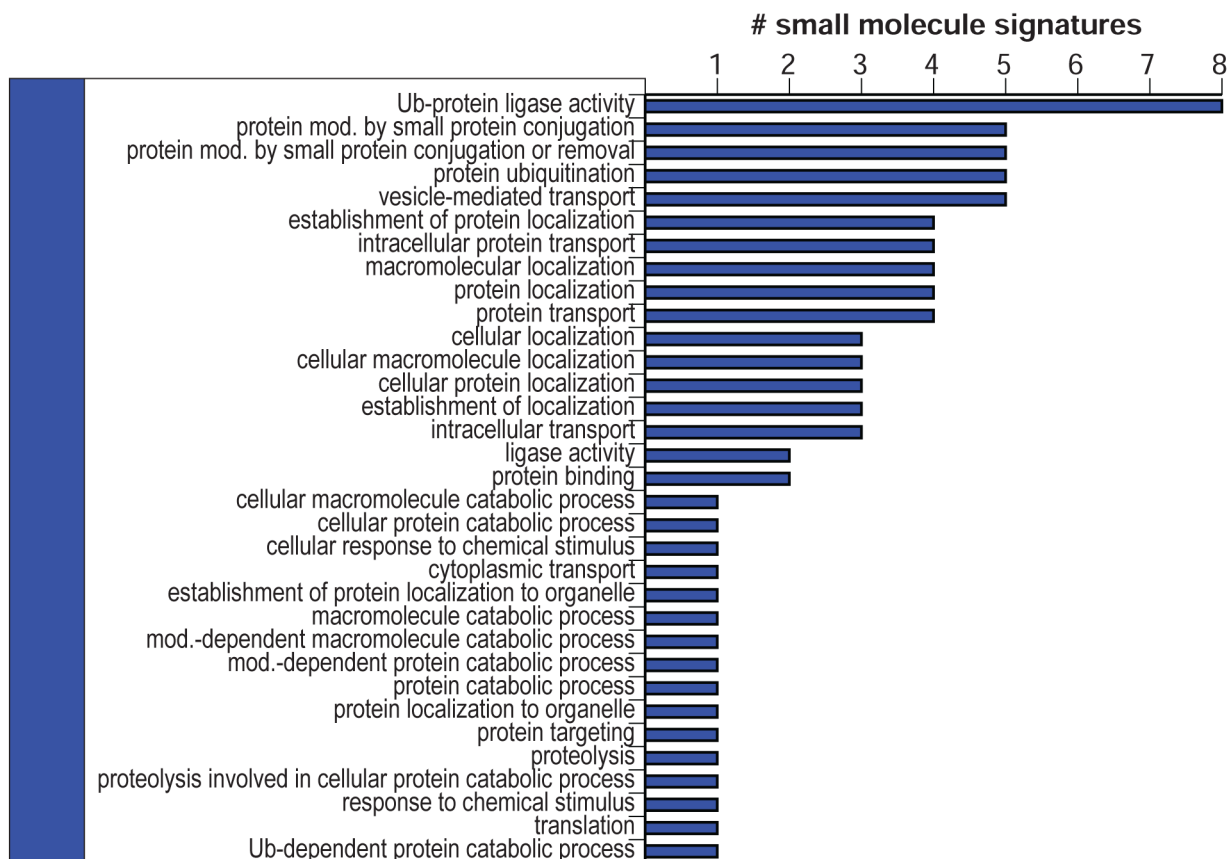


**Figure 2. Determinants of compound sensitivity**

We calculated whether molecules elicited a significant response from *C. neoformans* ORFs that are enriched for association with specific GO terms. Terms are listed on the y-axis and the number of compounds whose responding gene knockouts associated with that GO term are listed on the x-axis. See also Table S6.

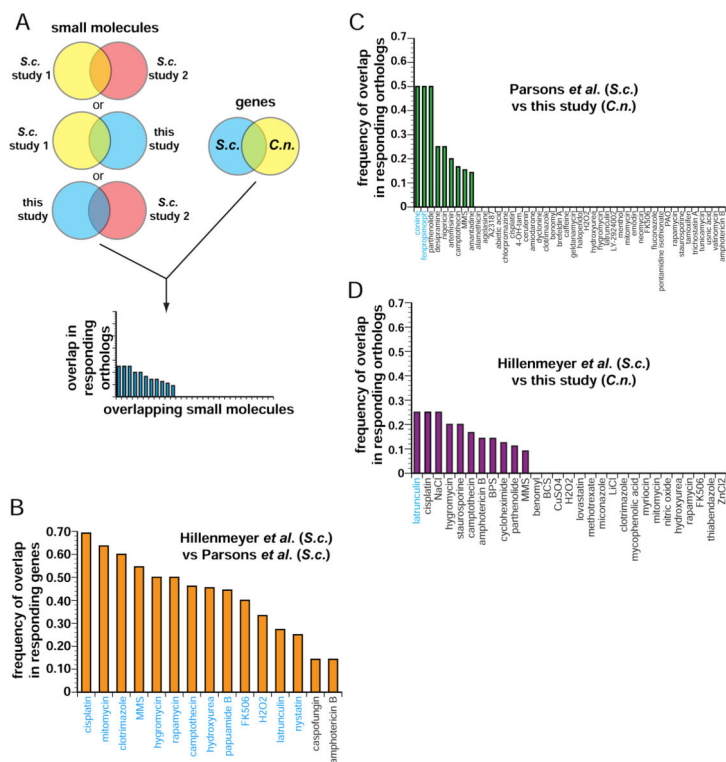


**Figure 3. Chemical-genetic signatures of *C. neoformans* genes differ from orthologous *S. cerevisiae* genes**

A) Flowchart of computation process for comparing datasets. We identified *C. neoformans* and *S. cerevisiae* orthologous genes that were present in all datasets, then compared the responses of only those genes in all the datasets. We compared genes whose knockout mutants significantly ( $|Z| > 2.5$ ) responded to compound that were common in at least two of the datasets.

B) Comparison between Parsons *et al.* and Hillenmeyer *et al.*, comparing the response ( $|Z| > 2.5$ ) of genes that have orthologs present in the *C. neoformans* dataset. Compounds whose profiles exhibit significant overlaps ( $p < 0.05$ ) are labeled in blue.

C) Comparison between our dataset and Parsons *et al.* Compounds whose profiles exhibit significant overlaps ( $p < 0.05$ ) are labeled in blue.

D) Comparison between our dataset and Hillenmeyer *et al.* Compounds whose profiles exhibit significant overlaps ( $p < 0.05$ ) are labeled in blue.

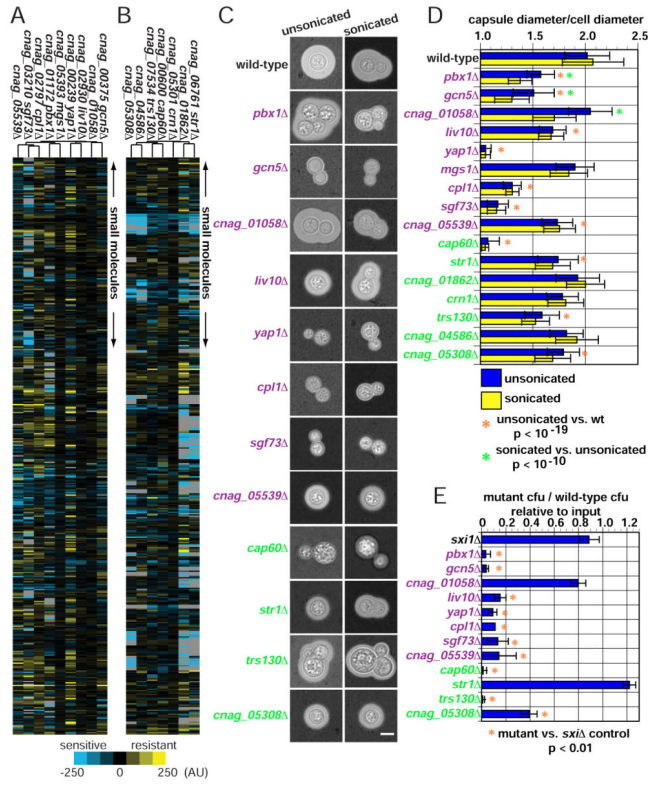


**Figure 4. Chemical-genetic profiling identifies genes involved in capsule biosynthesis**  
 A) Cluster containing the chemical signatures of the *pbx1* and *cpl1* mutants.  
 B) Cluster containing the chemical signatures of the *cap60* mutants.  
 C) Images of individual cells grown in 10% Sabouraud’s broth to induce capsule. Representative cells are shown for mutants that exhibit a statistically significant phenotype. Scale bar represents 5  $\mu$ m.  
 D) Quantification of capsule sizes from all mutants in *pbx1* /*cpl1* (purple labels) cluster or *cap60* (green labels) cluster. 100 cells were measured for each strain, the error bars represents the standard deviation, and p-values were calculated using Student’s t-test.  
 E) Colony counts from colony forming units (cfu) extracted from mouse lungs following an inhalation infection. Three mice are shown for each datapoint; the error bars represent the standard deviation and p-values were calculated using Student’s t-test.

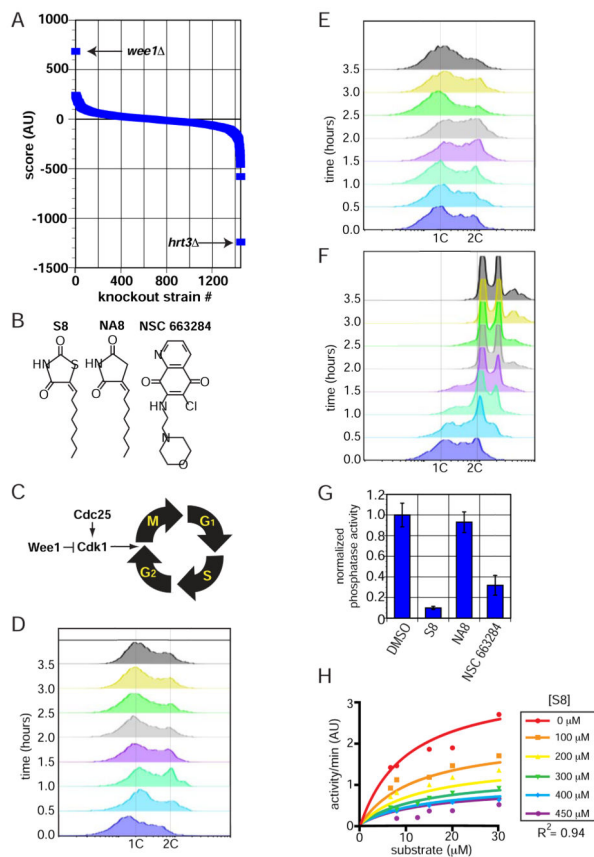


**Figure 5. *C. neoformans* Cdc25 is a target of S8 *in vivo* and *in vitro***

A) Chemical-genetic data of the growth scores of each knockout mutant grown on S8 (y-axis). The mutant that exhibited the greatest resistance is *wee1*. The mutant strain that showed the greatest sensitivity to S8 is *cnag\_04462*.

B) Structures of S8, NA8, and NSC 663284. The structure of S10 is shown in Fig. S3C.

C) G2/M regulation (Morgan, 2007).

D) DNA content of asynchronous *C. neoformans* culture split into aliquots for treatment with compounds of interest, with samples harvested at appropriate times. Data for DMSO-treated culture is shown.

E) DNA content from NA8-treated culture from same starting culture as Fig. 5F.

F) DNA content from S8-treated culture from same starting culture as Fig. 5F.

G) Phosphatase activity of purified *C. neoformans* Cdc25 catalytic domain (*CNAG\_01572*, aa442–662).

H) Michaelis-Menten kinetics of S8 inhibition of *Cn*Cdc25 from *in vitro* phosphatase activity. A noncompetitive model of enzyme inhibition produced the best R<sup>2</sup> value (0.94).

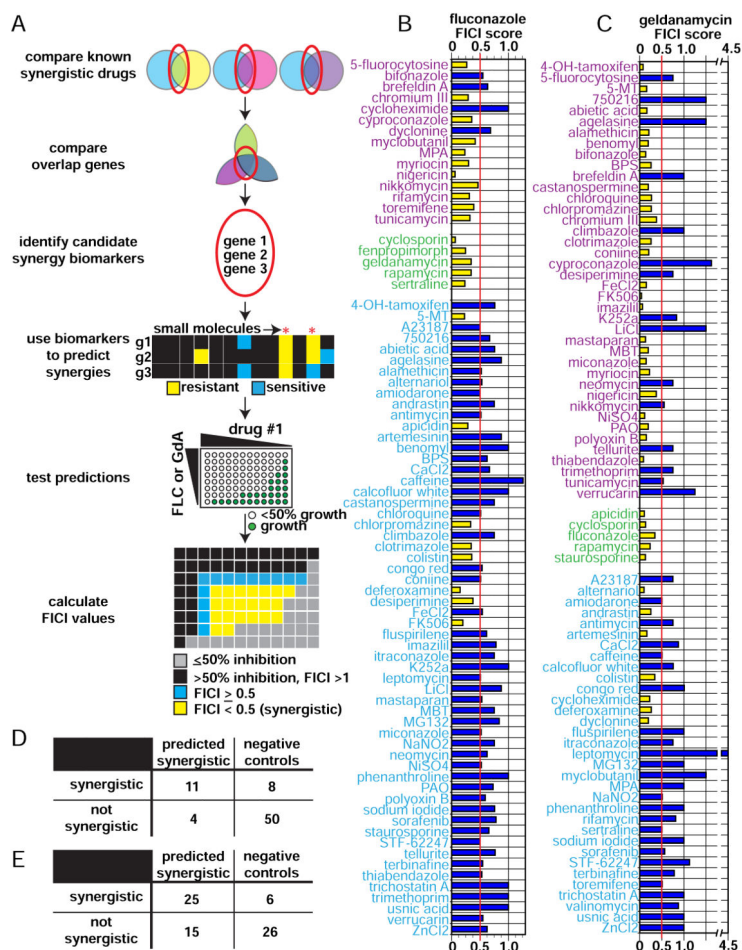


**Figure 6. O2M approach for predicting compound synergy**

A) Approach for predicting compound synergistic interaction.

B) FICI values for fluconazole (FLC). Predicted synergistic compounds are labeled in purple and known synergistic compounds in green. Bars represent the average of two assays but both had to be FICI < 0.5 to be considered synergistic. Compounds labeled in blue are negative controls from one of two categories: 1) predicted to synergize with geldanamycin (GdA) but not FLC or 2) randomly generated list of compounds not predicted to be synergistic with either FLC or GdA. Yellow bars represent an FICI < 0.5 (synergistic) and blue bars and FICI = 0.5 (not synergistic).

C) FICI values for GdA. Labels and colors are analogous to those in part B.

D) Contingency table of synergistic vs non-synergistic interactions with FLC.  $p < 0.0008$  (Fisher's exact test).

E) Contingency table of synergistic vs non-synergistic interactions with GdA.  $p < 0.0008$  (Fisher's exact test).



Table 1

## Small molecules and targets

A list of compounds used in this study, their targets, and the screening concentration.

Inhibitor (Activator)	Highest screening conc.	Process/enzyme	Category	Pubchem ID	FDA approval?
1-10 phenanthroline hydrochloride monohydrate	2uM	broad/transition metal complexes	broad spectrum	2723715	no
2-aminobenzothiazole	30uM	cytoskeleton function/kinesin Kip1	cell structure	8706	no
2-hydroxyethylhydrazine	0.156%	lipid synthesis/phospholipid methylation	lipid biosynthesis	8017	no
3-aminotriazole	6.25mM	histidine synthesis/IMP dehydratase	metabolism	1639	no
4-hydroxytamoxifen	1.56uM	estrogen receptor (mammals)	signaling	449459	yes
5-fluorocytosine	2.5ug/ml	DNA/RNA biosynthesis	DNA homeostasis/protein synthesis	3366	yes
5-methyltryptophan	8mM	tryptophan synthesis	metabolism	150990	no
abietic acid	1mM	lipid synthesis/lipoxygenase	lipid biosynthesis	10569	no
acifluorfen methyl (aconitine)	156.25ng/ml	porphyrin synthesis/protoporphyrinogen oxidase	metabolism	91642	no
aflatoxin B1	200ug/ml	membrane potential/Na <sup>+</sup> channels (mammals)	membrane polarization	245005	no
agelastine D	100ug/ml	DNA damaging agent	DNA homeostasis	14403	no
alantoin	5ug/ml	membrane potential/Na <sup>+</sup> /K <sup>+</sup> -ATPase (mammals)	membrane polarization	46231918	no
alantoin/U-22324	60uM	membrane integrity/forms a voltage-dependent ion channel	membrane polarization	16132042	no
alexidine dihydrochloride	125ug/ml	anti-microbial/mitochondria	mitochondria	102678	yes
allantoin	100ug/ml	nitrogen-rich compound	metabolism	204	topical
altamariol	2.5ug/ml	cholinesterase inhibitor/sodium channel activator and DNA supercoiling/topoisomerase I	broad spectrum	5359485	no
aluminum sulfate	1.5625mM	unknown	unknown	24850	no
(amantadine hydrochloride)	1.25mM	neurotransmitter release/glutamate receptor	signaling	64150	yes
amiodarone	60ug/ml	membrane potential/Na <sup>+</sup> /K <sup>+</sup> -ATPase (mammals)	membrane polarization	2157	yes
(ammonium persulfate)	50mM	reactive oxygen species	apoptosis/stress response/damage response	62648	no
amphotericin B	1ug/ml	lipid biosynthesis/ergosterol	membrane integrity	5280965	yes
andrastin A	4ug/ml	protein modification/farnesyltransferase	protein trafficking	6712564	no
anisomycin	50uM	translation/peptidyl transferase	gene expression	253602	no
antimycin	100ug/ml	respiration/cytochrome B	metabolism	14957	no

Inhibitor (Activator)	Highest screening conc.	Process/enzyme	Category	Pubchem ID	FDA approval?
apicidin	312.5ng/ml	chromatin regulation/HDACs	gene expression	6918328	no
artemisinin	312.5mM	iron metabolism/hematin detoxification	metabolism	68827	yes
ascomycin	3.125uM	signaling/calcineurin	signaling	6437370	yes
azide	62.5uM	respiration/cytochrome C oxidase	metabolism	33558	no
barium chloride	16mM	metal homeostasis/diverse	broad spectrum/unknown	25204	no
bafilomycin	4ug/ml	autophagy/vacuolar-type H <sup>+</sup> -ATPase	protein turnover	6436223	no
bathocuproine disulphonic acid (BCS)	3mM	copper acquisition	metabolism	16211287	no
bathophenanthroline disulfonate (BPS)	300uM	iron acquisition/Fe3-Ftr1	metabolism	65368	no
benomyl	100ug/ml	cytoskeleton function/tubulin	cell structure	28780	no
(betulinic acid)	64ug/ml	protein degradation/proteasome	protein turnover	64971	no
bifonazole	50ug/ml	lipid biosynthesis/HMG-CoA and ergosterol biosynthesis	membrane integrity	2378	no
brefeldin A	40ug/ml	ER-Golgi Transport/ARF GEF	secretion	5287620	no
calcium chloride	16mM	metal homeostasis/diverse	broad spectrum	5284359	no
caffeine	2.5mM	DNA damage checkpoint/ATM	DNA homeostasis	2519	no
calcium ionophore A23187	2.5ug/ml	membrane integrity/peptide that acts as ionophore	membrane integrity	40486	no
calcofluor white	500ug/ml	cell wall synthesis/chitin and cellulose	cell wall	6108780	no
camptothecin	500ug/ml	DNA supercoiling/topoisomerase I	DNA homeostasis	24360	analog
castanospermine	2.4mM	protein modification/glycosidation	protein modification	54445	derivative
cadmium chloride	1mM	metal homeostasis/diverse	broad spectrum/un known	24947	no
cerulenin	312.5ng/ml	fatty acid synthesis/beta-ketoacyl-acyl carrier protein synthase	lipid biosynthesis	5282054	no
cesium chloride	128mM	metal homeostasis/diverse	broad spectrum/unknown	24293	no
chlorpromazine hydrochloride	1.5625uM	phenothiazine antipsychotic drug (mammals)/dopamine, serotonin, and other neuroreceptors	signaling	6240	yes
chromium (III) chloride	8mM	metal homeostasis/diverse	broad spectrum	16211596	no
ciclopirox olamine	750ng/ml	iron acquisition and other	metabolism	38911	yes
cisplatin	100ug/ml	DNA synthesis	DNA homeostasis	157432	yes
climbazole	0.03125%	lipid biosynthesis/ergosterol biosynthesis and respiration/cytochrome P450	broad spectrum	37907	topical
clotrimazole	500mM	lipid biosynthesis/ergosterol biosynthesis	membrane integrity	2812	yes

Inhibitor (Activator)	Highest screening conc.	Process/enzyme	Category	Pubchem ID	FDA approval?
colistin	1mg/ml	membrane integrity	membrane integrity	5311054	yes
congo red	0.0625%	cell wall synthesis/chitin, cellulose, and glucan	cell wall	11313	no
conine	0.15625%	neurosignaling (mammals)/nicotinic receptor	signaling	441072	no
(crystal violet)	0.0012500%	oxidative stress inducer	stress response	11057	topical
CuCl <sub>2</sub>	8mM	copper homeostasis/diverse	metabolism	24014	no
cycloheximide	1.875ug/ml	translation/ribosome	gene expression	6197	no
cyclopiazonic acid	15.625uM	ion transport and cell polarization (mammals)/Ca <sup>2+</sup> -ATPase	metabolism	54682463	no
cyclosporin	75ug/ml	signaling/calcineurin	signaling	5284373	yes
cyproconazole	1.5625ug/ml	lipid biosynthesis/ergosterol biosynthesis	membrane integrity	86132	no
cyprodinil	10ug/ml	methionine biosynthesis	metabolism	86367	no
daphnetin	100uM	signaling/PKA, PKC, EGR receptor, others	signaling	5280569	no
desipramine hydrochloride	250uM	neurosignaling (mammals)/norepinephrine transporter	signaling	65327	yes
dyclonine hydrochloride	3.125uM	lipid biosynthesis/ergosterol biosynthesis	membrane integrity	68304	yes
emetine dihydrochloride hydrate	5mM	translation/ribosome	gene expression	3068143	yes
emodin	62.5uM	signaling/CK2, others	signaling	3220	yes
erlotinib	50ug/ml	signaling (mammals)/EGFR tyrosine kinase	signaling	176870	yes
FeCl <sub>3</sub>	32mM	iron acquisition, metal homeostasis	metabolism	24380	no
fenoxamil	80ug/ml	melanin biosynthesis	metabolism	11262655	no
fenpropimorph	2.5ug/ml	sterol synthesis	lipid biosynthesis	93365	no
FK506	312.5ng/ml	signaling/calcineurin	signaling	445643	yes
fluconazole	10ug/ml	lipid biosynthesis/ergosterol biosynthesis	membrane integrity	3365	yes
fluspirilene	25uM	antipsychotic drug, mechanism of action unknown	unknown	3396	yes
gallium (III) nitrate	25mM	metal homeostasis/diverse	broad spectrum	57352728	no
geldanamycin	2uM	protein folding/Hsp90	protein folding	5288382	trials
(H <sub>2</sub> O <sub>2</sub> )	6mM	reactive oxygen species	apoptosis/stress response/damage response	784	topical
haloperidol	125uM	phenothiazine antipsychotic drug (mammals)/dopamine, seratonin, and other neuroreceptors	signaling	3559	yes
harmine hydrochloride	1mM	cell differentiation (mammals)/PPARgamma	signaling	5359389	yes
hydroxyurea	12.5mM	DNA replication/replication fork progression	DNA homeostasis	3657	yes

Inhibitor (Activator)	Highest screening conc.	Process/enzyme	Category	Pubchem ID	FDA approval?
hygromycin	37.5ug/ml	translation/ribosome	gene expression	35766	no
imazalil	25ug/ml	lipid biosynthesis/ergosterol synthesis	membrane integrity	37175	no
iodoacetate	500uM	protein degradation/cysteine peptidases	protein turnover	5240	no
itraconazole	1.5625ug/ml	lipid biosynthesis/ergosterol synthesis	membrane integrity	55283	yes
K252a	10ug/ml	signaling/variety of kinases	signaling	127357	trials
latrunculin	25uM	cytoskeleton function/actin	cell structure	445420	no
lead (II) nitrate	64mM	metal homeostasis/diverse	broad spectrum	24924	no
leptomycin	1.25ug/ml	nucleocytoplasmic transport/Crm1	gene expression	6917907	no
LiCl	37.5mM	metal homeostasis/diverse	broad spectrum/un known	433294	no
lovastatin	37.5ug/ml	sterol synthesis/HMG CoA reductase	metabolism	53232	yes
LY 294002	375uM	signaling/PI3K	signaling	3973	no
magnesium chloride	150mM	metal homeostasis/diverse	broad spectrum	21225507	no
malachite green	3.125ug/ml	anti-microbial/unknown	anti-microbial	11294	no
manganese sulfate	128mM	metal homeostasis/diverse	metabolism	177577	no
mastoparan	5uM	signaling/G-proteins	signaling	5464497	no
(menadione)	150uM	vitamin K3/reactive oxygen species	diverse	4055	yes
menthol	1mM	voltage-dependent ion channels (mammals)/sodium channel	signaling	16666	yes
methotrexate	2.5uM	folate synthesis/DHFR	metabolism	126941	yes
methyl methanesulfonate (MMS)	0.0165%	DNA replication/replication fork progression	DNA homeostasis	4156	no
methylbenzethonium chloride (MBT)	0.25%	anti-microbial	anti-microbial	5702238	topical
MG132	12.5uM	protein degradation/proteasome	protein turnover	462382	no
miconazole	6.25ug/ml	lipid biosynthesis/ergosterol synthesis	membrane integrity	4189	yes
mitomycin C	12uM	DNA damaging agent	DNA homeostasis	5746	yes
myclobutamil	2ug/ml	lipid biosynthesis/ergosterol synthesis	membrane integrity	6336	no
mycophenolic acid	2.5ug/ml	GMP synthesis/IMP dehydrogenase	metabolism	446541	yes
myriocin	12.5ug/ml	sphingolipid synthesis	metabolism	6438394	analog
NA8		unknown	unknown		no
(NaCl)	37.5mM	osmotic regulation/HOG pathway	stress response	5234	yes
(NaNO2)	150uM	reactive nitrogen species	stress response	23668193	no

Inhibitor (Activator)	Highest screening conc.	Process/enzyme	Category	Pubchem ID	FDA approval?
neomycin sulfate	2.4mM	protein synthesis/ribosome	gene expression	8378	yes
nicotinamide	25uM	chromatin regulation/sirtuins	gene expression	936	yes
nigericin	100ug/ml	membrane integrity/ion gradient	membrane polarization	34230	no
nikkomyacin	5ug/ml	chitin synthesis	cell wall	72479	no
NISO4	1mM	anti-fungal/diverse	anti-fungal	5284429	no
nocodazole	30uM	cytoskeleton function/tubulin	cell structure	4122	no
ophiobolin A	62.5ng/ml	signaling/calmodulin	signaling	5281387	no
parthenolide	150uM	immune and inflammatory response/NF-kB	signaling	6473881	no
pentamidine isethionate	500uM	anti-microbial/mitochondrial function	anti-microbial	8813	yes
pH	8.0, 8.5, 9.0	pH homeostasis	diverse		no
phenylarsine oxide	2.5uM	broad/XCCX protein phosphatases	broad spectrum	4778	no
picoxystrobin	6.25ug/ml	quinone outside inhibitor class/fungal cytochrome bcl	mitochondria	11285653	no
(plumbagin)	2.8uM	reactive oxygen species	stress response	10205	no
PMSF	10mM	vacuolar proteolysis/proteinase B	signaling	4784	no
polyoxin B	200ug/ml	chitin synthesis	cell wall	3084093	no
povidone iodine	2%	anti-microbial	anti-microbial	410087	topical
prussian blue	75mM	monocation chelator	metabolism	16211064	yes
quimic acid	2mM	anti-microbial	anti-microbial	6508	no
rapamycin	0.125uM	signaling/TOR kinases	signaling	5284616	yes
rubidium chloride	150mM	potassium metabolism/competitor	metabolism	62683	no
rifamycin SV monosodium salt	200ug/ml	RNA synthesis/RNA polymerase	gene expression	6324616	yes
S10		unknown	unknown		no
S8		unknown	unknown		no
S-aminoethyl-L-cysteine (thialysine)	10uM	amino acid metabolism/lysine analog	metabolism	20048	no
SDS	0.0015625 %	cell membrane integrity	membrane integrity	3423265	no
selumetinib	150ug/ml	signaling/MAPK (ERK)	signaling	10127622	no
sertraline	15ug/ml	neurosignaling (mammals)/serotonin reuptake	neurosignaling	68617	yes
sodium azide	62.5uM	respiration/cytochrome oxidase	mitochondria	33557	no
sodium borate	10mM	anti-microbial/diverse	anti-microbial	21749317	no

Inhibitor (Activator)	Highest screening conc.	Process/enzyme	Category	Pubchem ID	FDA approval?
sodium hydrosulfite	6.25mM	anti-microbial, counteracts some anti-microbials	anti-microbial	24489	no
sodium iodide	75mM	anti-microbial	anti-microbial	5238	yes
sodium metavanadate	10mM	signaling/protein phosphotyrosine phosphatases	signaling	4148882	no
(sodium molybdate)	64mM	respiration/oxygen uptake	diverse	61424	no
sodium selenite	4mM	respiration/oxygen uptake	diverse	16210997	yes
sodium sulfite	100mM	ATP synthesis and accumulation/unknown	metabolism	24437	no
sodium tungstate	64mM	metal homeostasis/diverse	broad spectrum/unknown	150191	no
sorafenib	100uM	signaling/VEGF tyrosine kinase	signaling	216239	yes
staurosporine	3uM	signaling/PKC1	signaling	5279	yes
(STF-62247)	400uM	autophagy	protein turnover	704473	trials
sulfometuron methyl	100ug/ml	branch chain amino acid synthesis/acetolactate synthase	metabolism	52997	no
suloctidil	400uM	Ca2+ homeostasis in blood vessels (mammals)/putative Ca2+ channel blocker	vascular system/metabolism	5354	formerly
tamoxifen citrate	10uM	estrogen signaling (mammals)/estrogen receptor, mixed agonist/antagonist	signaling	2733525	yes
tauridine	0.01%	anti-microbial/lipopolysaccharide detection and signaling	host defense	29566	yes
tautomycin	250nM	signaling/PP2A	signaling	3034761	no
tellurite	0.1%	sulfate assimilation	metabolism	115037	no
terbinafine	75uM	sterol synthesis/squalene epoxidase	metabolism	1549008	yes
thiabendazole	200ug/ml	respiration/NADH oxidase	mitochondria	5430	yes
thonzonium bromide	25uM	anti-microbial, pH homeostasis/V-ATPase	broad spectrum	11102	yes
tomatine	5ug/ml	glycoalkaloid anti-fungal of unknown mechanism/ergosterol biosynthesis	anti-fungal/membrane integrity	28523	no
trichostatin A	100uM	chromatin regulation/HDACs	gene expression	444732	no
trifluoperazine	200uM	signaling/calmodulin	signaling	5566	yes
trimethoprim	1.6mg/ml	folate synthesis/DHFR	metabolism	5578	yes
tunicamycin	2.5ug/ml	glycosylation/Alg7	secretion	11104835	no
usnic acid	25ug/ml	anti-microbial	anti-microbial	6433557	trials
valinomycin	20uM	membrane integrity/potassium exclusion	membrane polarization	5649	no
verrucairin	5uM	protein biosynthesis/polysome	protein turnover	6437060	no

Inhibitor (Activator)	Highest screening conc.	Process/enzyme	Category	Pubchem ID	FDA approval?
ZnCl <sub>2</sub>	4mM	metal homeostasis/diverse	diverse	5727	no

Brown et al.